Applications and Applied Mathematics: An International Journal (AAM)

Volume 16 | Issue 1 Article 28

6-2021

Casson Fluid Flow Past on Vertical Cylinder in the Presence of Chemical Reaction and Magnetic Field

Gaurav Kumar
Babu Banarasi Das University

S.M.K. Rizvi
Babu Banarasi Das University

Available at
http://pvamu.edu/aam
Appl. Appl. Math.
ISSN: 1932-9466

Applications and Applied Mathematics:
An International Journal
(AAM)

Vol. 16, Issue 1 (June 2021), pp. 524 – 537

Casson Fluid Flow Past on Vertical Cylinder in the Presence of Chemical Reaction and Magnetic Field

[1*]Gaurav Kumar and [2]S.M.K. Rizvi

Department of Mathematics & Computer Science
Babu Banarasi Das University
Lucknow, U.P., India
[1]logontogauravsharma@gmail.com; [2]kamil@bbdu.ac.in

[*]Corresponding author

Received: October 9, 2020; Accepted: April 25, 2021

Abstract

In this paper, we have examined the behavior of unsteady flow of a viscous, incompressible and electrically conducting Casson fluid past an impulsively started vertical cylinder with variable temperature and mass diffusion in the presence of transversely applied uniform magnetic field and chemical reaction. The temperature and concentration level near the surface increase linearly with time. The governing equations of non-dimensional form of flow model have been solved numerically by using Crank-Nicolson implicit finite difference method. The velocity profile is discussed with the help of graphs drawn for different parameters like Casson fluid parameter, Prandtl number, chemical reaction parameter and the magnetic field parameter. The numerical values obtained for skin-friction, Nusselt number and Sherwood number have been tabulated. It is seen that the values obtained for velocity, concentration and temperature are in concurrence with the actual flow of the Casson fluid. The importance of the problem can be seen in the manufacturing of pharmaceutical products, coal in water, paints, and synthetic lubricants etc.

Keywords: MHD flow; chemical reaction; Casson fluid; mass diffusion; vertical cylinder; finite difference; skin-friction

MSC 2010 No.: 76W05, 76D05, 80A20

1. Introduction

MHD fluid flow with heat and mass transfer of a viscous fluid past in cylinder is a significant problem in fluid dynamics. Casson fluid is another fluid model for non-Newtonian fluid. The most important non-Newtonian fluid possessing a yield value is the Casson fluid, which are carried significant application in polymer processing industries and biomechanics. Casson fluid

is a shear thinning liquid which has an infinite viscosity at a zero rate of strain. Casson fluid equations demonstrate a nonlinear relationship between stress and rate of strain. It has been found to be accurately and significantly applicable to silicon suspension, suspensions of benthic in water. The Casson fluid model is sometimes stated to fit rheological data better than general viscoplastic models for many materials. The non-linear Casson's constitutive equation has been found to describe accurately the flow curves of suspensions of pigments in lithographic varnishes used for preparation of printing inks. In the literature, Unsteady MHD Casson fluid flow through a parallel plate with Hall current was investigated by Afikuzzaman et al. (2014) and they have used explicit finite difference technique to solve the momentum and energy equation.

Heat and mass transfer in magnetohydrodynamic Casson fluid flow past over an oscillating vertical plate embedded in porous medium with ramped wall temperature was studied by Kataria and Patel (2018). They discussed that velocity increases with increasing values of Casson parameter and the velocity boundary layer thickness for Casson fluid is larger than the Newtonian fluid. It occurs because of plasticity of Casson fluid. The plasticity of the fluid increases with decrease in Casson parameter. It causes the increment in velocity boundary layer thickness. Rajput and Kumar (2016) have investigated unsteady MHD flow in porous media past over exponentially accelerated inclined plate with variable wall temperature and mass transfer along with Hall current. Further, they (2016) have worked on effects of radiation and chemical reaction on MHD flow past a vertical plate with variable temperature and mass diffusion. Animasaun et al. (2016) have worked on Casson fluid flow with variable thermo-physical property along exponentially stretching sheet with suction and exponentially decaying internal heat generation using the homotopy analysis method. They have discussed that an increase in the variable plastic dynamic viscosity parameter of Casson fluid corresponds to an increase in the velocity profiles and a decrease in temperature throughout the boundary layer. Ghalambaz et al. (2019) have investigated MHD natural convection of Cu–Al2O3 water hybrid nanofluids in a cavity equally divided into two parts by a vertical flexible partition membrane. Chamkha et al. (2013) have worked on radiation effects on mixed convection about a cone embedded in a porous medium filled with a nanofluid. Eugen and chamkha (2010) have presented combined effect of heat generation or absorption and first-order chemical reaction on micropolar fluid flows over a uniformly stretched permeable surface. Pramanik (2014) has solved numerically fluid model based on Casson fluid flow and heat transfer past an exponentially porous stretching surface in presence of thermal radiation. Heat and mass transfer in unsteady MHD Casson fluid flow with convective boundary conditions was presented by Pushpalatha et al. (2016) and they have analytically solved governing equations of the flow model by using perturbation technique.

Examples of Casson fluids are jelly, tomato sauce, honey, soup, and concentrated fruit juices, etc. Human blood can also be treated as Casson fluid. Due to the presence of several substances like, protein, fibrinogen and globulin in aqueous base plasma, human red blood cells can form a chainlike structure, known as aggregates or rouleaux. An approximate Casson fluid model for tube flow of blood was explained by Walwander et al. (1975). Das and Batra (1993) have investigated secondary flow of a Casson fluid in a slightly curved tube. MHD Casson fluid flow past a non isothermal porous linearly stretching sheet was examined by Wahiduzzaman et al. (2014). Transient MHD Couette flow of a Casson fluid between parallel plates with heat transfer were studied by Hazem and Mohamed (2010). Effect of aligned magnetic field on Casson fluid flow past a vertical oscillating plate in porous medium was presented by Reddy et al. (2016). Hall current effect on chemically reacting MHD Casson fluid flow with Dufour effect and thermal radiation was considered by Vijayaragavan and Karthikeyan (2018). Husein

et al. (2019) have worked on numerical solution of heat transfer in MHD mixed convection flow micro-polar Casson fluid about solid sphere with radiation effect. Kumar et al. (2019) have demonstrated chemical reaction effect on MHD flow past an impulsively started vertical cylinder with variable temperature and mass diffusion. Further, Kumar along with Bansal (2019) have developed unsteady flow past on vertical cylinder in the presence of an inclined magnetic field and chemical reaction. Takhar et al. (2000) have examined combined heat and mass transfer along a vertical moving cylinder with a free stream. Further, they (2001) have worked on unsteady three-dimensional MHD boundary layer flow due to the impulsive motion of a stretching surface. MHD flow past on a plate with heat transfer was studied by us along with Rajput (2016) and (2018) in different parameter.

The MHD Casson fluid flow model under consideration analyzes the effect of chemical reaction. In this paper, the fluid flow problem is solved numerically using Crank-Nicolson implicit finite difference technique. A selected set of graphical results illustrating the effects of various parameters involved in the problem are presented and discussed. The numerical values of skin-friction, local Nusselt number and Sherwood number have been tabulated.

2. Mathematical Analysis

The geometrical model of the problem is shown in Figure-A.

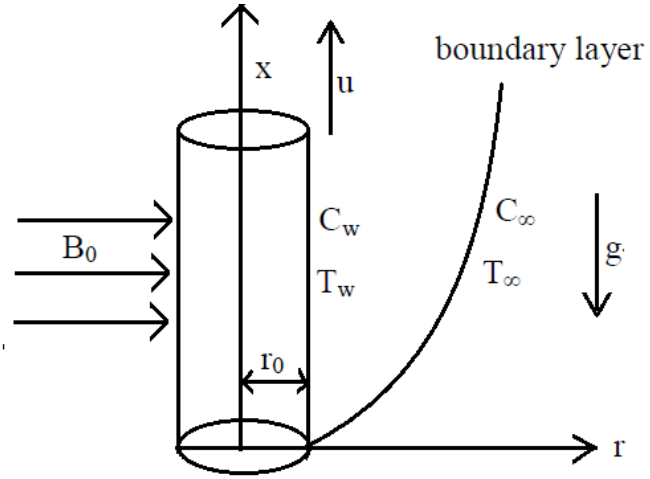

Figure-A. Physical model of the flow

Consider an unsteady flow of an incompressible viscous electrically conducting fluid mixture past an impulsively started semi-infinite vertical cylinder of radius r_0. Here, the x-axis is taken along the axis of cylinder in the vertical direction and the radial coordinate r is taken normal to the cylinder. The gravitational acceleration g is acting downward. The magnetic field B_0 of uniform strength is applied perpendicular to the flow. During the motion, the direction of the magnetic field changes along with the plate in such a way that it always remains perpendicular to it. This means, the direction of magnetic field is tied with the surface. Initially it has been considered that the surface of the cylinder as well as the fluid is at the same temperature T_∞. The species concentration in the fluid is taken as C_∞ for all $t \leq 0$. At time $t > 0$, the cylinder starts moving with a velocity u_0 in its own plane and temperature of the surface of the cylinder is raised to T_w. The concentration C_w near the surface is raised linearly with respect to time.

The rheological equation of state for the Cauchy stress tensor of Casson fluid is written as,

$$\tau = \tau_0 + \mu\alpha^*, \tag{1}$$

equivalently,

$$\tau_{ij} = \begin{cases} 2\left(\mu_B + \dfrac{p_y}{\sqrt{2\pi}}\right)e_{ij}, & \pi > \pi_c, \\ 2\left(\mu_B + \dfrac{p_y}{\sqrt{2\pi_c}}\right)e_{ij}, & \pi < \pi_c, \end{cases} \tag{2}$$

where, τ is shear stress, τ_0 is Casson yield stress, μ is dynamic viscosity, α^* is shear rate, τ_{ij} is the $(i, j)^{th}$ component of stress tensor. π is the product of the component of deformation rate with itself that is $\pi = e_{ij}e_{ij}$ and e_{ij} is the $(i, j)^{th}$ component of deformation rate, π_c is a critical values of this product based on the non-Newtonian fluid model. μ_B is plastic dynamic viscosity of the non-Newtonian fluid.

$$p_y = \frac{\mu_B\sqrt{2\pi}}{\gamma}, \tag{3}$$

where p_y denote the yield stress of fluid. So, if a shear stress less than the yield stress is applied to the fluid. It behaves like a solid, whereas if a shear stress greater than yield stress is applied, it starts to move. Some fluids require a gradually increasing shear stress to maintain a constant strain rate and are called Rheopectic, in the case of Casson fluid (Non-Newtonian) flow where $\pi > \pi_C$,

$$\mu = \mu_B + \frac{p_y}{\sqrt{2\pi}}. \tag{4}$$

Using the equations (3) and (4), then the kinematic viscosity can be written as,

$$\upsilon = \frac{\mu}{\rho} = \frac{\mu_B + \dfrac{p_y}{\sqrt{2\pi}}}{\rho} = \frac{\mu_B}{\rho}\left(1 + \frac{1}{\gamma}\right). \tag{5}$$

Taking into consideration the above assumptions and the Boussinesq's approximation, the flow is governed by the following system of equations:

$$\frac{\partial u}{\partial t} = \upsilon\left(1 + \frac{1}{\gamma}\right)\frac{\partial^2 u}{\partial r^2} + \frac{\upsilon}{r}\left(1 + \frac{1}{\gamma}\right)\frac{\partial u}{\partial r} + g\beta\,(T - T_\infty) + g\beta^*\,(C - C_\infty) - \frac{\sigma B_0^2 u}{\rho}, \tag{6}$$

$$\frac{\partial T}{\partial t} = \alpha\frac{\partial^2 T}{\partial r^2} + \frac{\alpha}{r}\frac{\partial T}{\partial r}, \tag{7}$$

$$\frac{\partial C}{\partial t} = D\frac{\partial^2 C}{\partial r^2} + \frac{D}{r}\frac{\partial C}{\partial r} - K_C(C - C_\infty), \tag{8}$$

The initial and boundary conditions are:

$$\left.\begin{aligned} &t \le 0 : u = 0,\ T = T_\infty,\ C = C_\infty, \ \text{for every } r, \\ &t > 0 : u = u_0,\ T = T_\infty + (T_w - T_\infty)\frac{t\upsilon}{r_0^2},\ C = C_\infty + (C_w - C_\infty)\frac{t\upsilon}{r_0^2}, \ \text{at } r = r_0, \\ &u \to 0,\ T \to T_\infty,\ C \to C_\infty \ \text{as } r \to \infty. \end{aligned}\right\} \tag{9}$$

Here, u is the velocity of fluid, g-the acceleration due to gravity, β-volumetric coefficient of thermal expansion, t-time, T-temperature of the fluid, β^*-volumetric coefficient of concentration expansion, C- species concentration in the fluid, ν-the kinematic viscosity, ρ-the density, C_p- the specific heat at constant pressure, k- thermal conductivity of the fluid, D-the mass diffusion coefficient, T_w-temperature of the plate at $z= 0$, C_w-species concentration at the plate $z= 0$, B_0 - the uniform magnetic field, K_c-chemical reaction, σ-electrical conductivity.

The following non-dimensional quantities are introduced to transform equations (6), (7) and (8) into dimensionless form:

$$\begin{aligned} &\mathrm{R} = \frac{\mathrm{r}}{\mathrm{r}_0},\ \bar{\mathrm{u}} = \frac{\mathrm{u}}{u_0},\quad \theta = \frac{(\mathrm{T} - \mathrm{T}_\infty)}{(\mathrm{T}_\mathrm{w} - \mathrm{T}_\infty)},\ \mathrm{S_c} = \frac{\upsilon}{\mathrm{D}},\ \mu = \rho\upsilon, \\ &\bar{\mathrm{C}} = \frac{(\mathrm{C} - \mathrm{C}_\infty)}{(\mathrm{C}_\mathrm{w} - \mathrm{C}_\infty)}, G_r = \frac{g\beta\upsilon(T_w - T_\infty)}{u_0\upsilon},\ \mathrm{M} = \frac{\sigma \mathrm{B}_0^2 r_0^2}{\upsilon\rho},\ \mathrm{P_r} = \frac{\upsilon}{\alpha}, \\ &\mathrm{G_m} = \frac{\mathrm{g}\beta^*\upsilon(\mathrm{C_w} - \mathrm{C}_\infty)}{u_0\upsilon},\ \mathrm{K}_0 = \frac{\upsilon K_C}{u_0^2},\ \gamma = \frac{\mu_B\sqrt{2\pi}}{p_y} \quad \bar{\mathrm{t}} = \frac{\mathrm{t}\upsilon}{\mathrm{r}_0^2}, \end{aligned} \tag{10}$$

where $\bar{u}$ is the dimensionless velocity, $\bar{t}$ - dimensionless time, θ - the dimensionless temperature, $\bar{C}$-the dimensionless concentration, G_r - thermal Grashof number, G_m- mass Grashof number, μ - the coefficient of viscosity, K_0 -chemical reaction parameter, P_r- the Prandtl number, S_c - the Schmidt number, γ- the Casson fluid parameter, M- the magnetic parameter.

The flow model in dimensionless form as:

$$\frac{\partial\bar{u}}{\partial\bar{t}} = \left(1 + \frac{1}{\gamma}\right)\frac{\partial^2\bar{u}}{\partial R^2} + \frac{1}{R}\left(1 + \frac{1}{\gamma}\right)\frac{\partial\bar{u}}{\partial R} + G_r\,\theta + G_m\,\bar{C} - M\bar{u}, \tag{11}$$

$$\frac{\partial\theta}{\partial\bar{t}} = \frac{1}{P_r}\frac{\partial^2\theta}{\partial R^2} + \frac{1}{R\,P_r}\frac{\partial\theta}{\partial R}, \tag{12}$$

$$\frac{\partial\bar{C}}{\partial\bar{t}} = \frac{1}{S_c}\frac{\partial^2\bar{C}}{\partial R^2} + \frac{1}{R\,S_c}\frac{\partial\bar{C}}{\partial R} - K_0\bar{C}. \tag{13}$$

The corresponding boundary conditions (9) become:

$$\left.\begin{array}{ll} \bar{t} \le 0 : \bar{u} = 0,\ \theta = 0,\ \bar{C} = 0, & \text{for every } R, \\ \bar{t} > 0 : \bar{u} = 1, \theta = \bar{t},\ \bar{C} = \bar{t}, & \text{at } R = 0, \\ \bar{u} \to 0,\ \theta \to 0,\ \bar{C} \to 0, & \text{as } R \to \infty. \end{array}\right\} \tag{14}$$

Dropping bars in the above equations, we get:

$$\frac{\partial u}{\partial t} = (1+\frac{1}{\gamma})\frac{\partial^2 u}{\partial R^2} + \frac{1}{R}(1+\frac{1}{\gamma})\frac{\partial u}{\partial R} + G_r\theta + G_m C - Mu, \tag{15}$$

$$\frac{\partial \theta}{\partial t} = \frac{1}{P_r}\frac{\partial^2 \theta}{\partial R^2} + \frac{1}{R\,P_r}\frac{\partial \theta}{\partial R}, \tag{16}$$

$$\frac{\partial C}{\partial t} = \frac{1}{S_c}\frac{\partial^2 C}{\partial R^2} + \frac{1}{R\,S_c}\frac{\partial C}{\partial R} - K_0 C. \tag{17}$$

The boundary conditions become:

$$\left.\begin{array}{ll} t \le 0 : u = 0,\ \theta = 0, C = 0, & \text{for every } R, \\ t > 0 : u = 1, \theta = t,\ C = t, & \text{at } R = 0, \\ u \to 0,\ \theta \to 0,\ C \to 0, & \text{as } R \to \infty. \end{array}\right\} \tag{18}$$

2. Method of solution

Equations (15) to (17) are non-linear partial differential equations are solved using boundary and initial conditions (18). These equations are solved by Crank- Nicolson implicit finite difference method for numerical solution. The finite difference equations corresponding to equations (15) to (17) are as follows:

$$\begin{aligned} u_i^{j+1} - u_i^j &= \frac{\Delta t}{2(\Delta R)^2}(1+\frac{1}{\gamma})(u_{i+1}^j - 2u_i^j + u_{i-1}^j + u_{i+1}^{j+1} - 2u_i^{j+1} + u_{i-1}^{j+1}) \\ &\quad + \frac{\Delta t}{4(1+(i-1)\Delta R)(\Delta R)}(1+\frac{1}{\gamma})(u_{i+1}^j - u_{i-1}^j + u_{i+1}^{j+1} - u_{i-1}^{j+1}) \\ &\quad + \frac{\Delta t G_r}{2}((\theta_i^{j+1} + \theta_i^j)) + \frac{\Delta t G_m}{2}(C_i^{j+1} + C_i^j) - \frac{\Delta t M}{2}(u_i^{j+1} + u_i^j). \end{aligned} \tag{19}$$

$$\begin{aligned} \theta_i^{j+1} - \theta_i^j &= \frac{\Delta t}{2\,P_r\,(\Delta R)^2}(\theta_{i+1}^j - 2\theta_i^j + \theta_{i-1}^j + \theta_{i+1}^{j+1} - 2\theta_i^{j+1} + \theta_{i-1}^{j+1}) \\ &\quad + \frac{\Delta t}{4\,P_r\,(1+(i-1)\Delta R)(\Delta R)}(\theta_{i+1}^j - \theta_{i-1}^j + \theta_{i+1}^{j+1} - \theta_{i-1}^{j+1}). \end{aligned} \tag{20}$$

$$\begin{aligned} C_i^{j+1} - C_i^j &= \frac{\Delta t}{2\,S_c\,(\Delta R)^2}(C_{i+1}^j - 2C_i^j + C_{i-1}^j + C_{i+1}^{j+1} - 2C_i^{j+1} + C_{i-1}^{j+1}) \\ &\quad + \frac{\Delta t}{4\,S_c\,(1+(i-1)\Delta R)(\Delta R)}(C_{i+1}^j - C_{i-1}^j + C_{i+1}^{j+1} - C_{i-1}^{j+1}) - \Delta t K_0 (C_i^{j+1} + C_i^j). \end{aligned} \tag{21}$$

Here, index i refers to R and j refers to time t, $\Delta t = t_{j+1} - t_j$ and $\Delta R = R_{j+1} - R_j$. Knowing the values of u, θ and C at time t, we can compute the values at time $t+\Delta t$ as follows: we substitute $i = 1, 2, ..., N-1$, where N correspond to ∞. The implicit Crank-Nicolson finite difference method

is a second order method ($o(\Delta t^2)$) in time and has no restriction on space and time steps, that is, the method is unconditionally stable. The computation is executed for $\Delta R = 0.1$, $\Delta t = 0.002$ and procedure is repeated till $R = 40$.

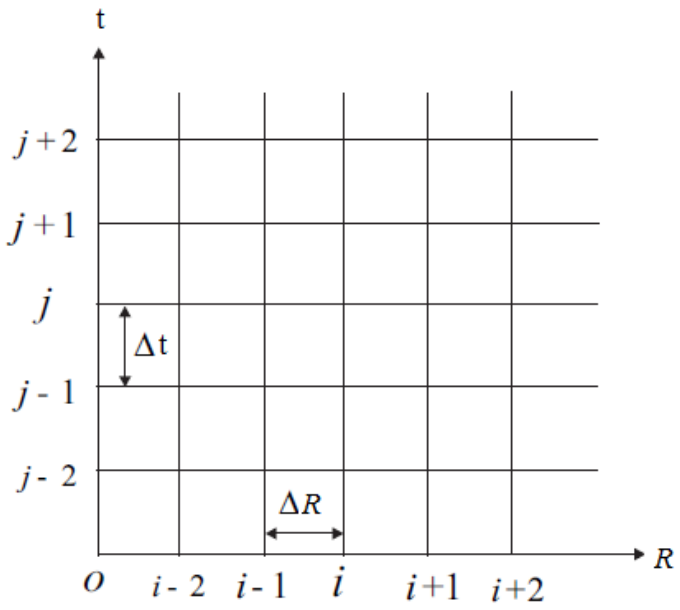

Figure-B. Finite Difference grids

The implicit method provides stable solutions of the problem and requires matrix inversions which we have done at step forward in time. Due to this problem is an initial-boundary value related problem with a finite number of spatial grid points. Therefore, the corresponding flow model equations do not automatically guarantee the convergence of the mesh $\Delta R \to 0$. To achieve maximum numerically efficiency, we have used the tri-diagonal procedure to solve the two- point conditions governing the main coupled governing equations of momentum and energy. The convergence (consistency) of the process is quite satisfactory and the numerical stability of the method is guaranteed by the implicit nature of the numerical scheme. Hence, the scheme is consistent. The stability and consistency ensure convergence.

Now it is important to calculate the physical quantities of primary interest, which are the local shear stress, local surface heat flux and Sherwood number.

2.1. Skin Friction

The dimensionless local wall shear stress or skin-friction at the surface is obtained as,

$$\tau = -\left(\frac{\partial u}{\partial R}\right)_{R=0}.$$

The numerical values of τ for different parameters are given in Table 1.

2.2. Nusselt number

The dimensionless local surface heat flux or Nusselt number at the surface is obtained as,

$$Nu = -\left(\frac{\partial \theta}{\partial R}\right)_{R=0}.$$

The numerical values of *Nu* for different parameters are given in Table 2.

2.3. Sherwood number

The dimensionless the local Sherwood number at the surface is obtained as,

$$Sh = -\left(\frac{\partial C}{\partial R}\right)_{R=0}.$$

The numerical values of S_h for different parameters are given in Table 3.

3. Stability Analysis

The stability criterion of the finite difference scheme for constant mesh sizes are analyzed by using Von-Neumann Technique. This technique was explained by Carnahan et al. (1969). In the Fourier expansion, the general term for *u, θ, C* at a time arbitrarily called *t=0*, are assumed to be of the form $e^{i\beta R}$ where $i = \sqrt{-1}$. At a later time, these terms will become,

$$u = \xi_1(t)\, e^{i\beta R}, \tag{22}$$

$$\theta = \xi_2(t)\, e^{i\beta R}, \tag{23}$$

$$C = \xi_3(t)\, e^{i\beta R}. \tag{24}$$

Putting equations (17)-(19) in equations (14)-(16) under the assumption that the coefficients *u, θ, C* as constants over any one time step and denoting the values after one time step by ξ_1', ξ_2' and ξ_3'. After simplification, we have

$$\begin{aligned}\frac{\xi_1'-\xi_1}{\Delta t} &= \frac{G_r(\xi_2'+\xi_2)+G_m(\xi_3'-\xi_3)}{2}+\left(1+\frac{1}{\gamma}\right)\frac{\{\cos(\beta\Delta R)-1\}}{(\Delta R)^2}(\xi_1'+\xi_1)\\ &\quad -\frac{M}{2}(\xi_1'+\xi_1)+\frac{i\sin(\beta\Delta R)}{2\Delta R(1+(i-1)\Delta R)}\left(1+\frac{1}{\gamma}\right)(\xi_1'+\xi_1),\end{aligned} \tag{25}$$

$$\frac{\xi_2'-\xi_2}{\Delta t} = \frac{(\xi_2'+\xi_2)}{\Pr}\left[\frac{\cos(\beta\Delta R)-1}{(\Delta R)^2}+\frac{i\sin(\beta\Delta R)}{2\Delta R(1+(i-1)\Delta R)}\right], \tag{26}$$

$$\frac{\xi_3'-\xi_3}{\Delta t} = \frac{(\xi_3'+\xi_3)}{Sc}\left[\frac{\cos(\beta\Delta R)-1}{(\Delta R)^2}+\frac{i\sin(\beta\Delta R)}{2\Delta R(1+(i-1)\Delta R)}\right]-K_0(\xi_3'+\xi_3). \tag{27}$$

Equations (25) to (27) can be rewritten as,

$$(1+F)\xi_1' = (1-F)\xi_1+\frac{G_r}{2}(\xi_2'+\xi_2)+\frac{G_m}{2}(\xi_3'+\xi_3), \tag{28}$$

$$(1+G)\xi_2' = (1-G)\xi_2, \tag{29}$$

$$(1+H)\xi_3' = (1-H)\xi_3. \tag{30}$$

Here,

$$F = \left(1+\frac{1}{\gamma}\right)\frac{\{1-\cos(\beta\Delta R)\}(\Delta t)}{(\Delta R)^2} + \frac{M(\Delta t)}{2} - \left(1+\frac{1}{\gamma}\right)\frac{(\Delta t)\, i\sin(\beta\Delta R)}{2\Delta R(1+(i-1)\Delta R)},$$

$$G = \frac{\{1-\cos(\beta\Delta R)\}(\Delta t)}{P_r(\Delta R)^2} - \frac{(\Delta t)\, i\sin(\beta\Delta R)}{2P_r\Delta R(1+(i-1)\Delta R)},$$

$$H = \frac{\{1-\cos(\beta\Delta R)\}(\Delta t)}{S_c(\Delta R)^2} - \frac{(\Delta t)\, i\sin(\beta\Delta R)}{2S_c\Delta R(1+(i-1)\Delta R)} + K_0(\Delta t).$$

Eliminating ξ_2' and ξ_3' in equation (28) by using (29) and (30). The resultant equation is of the form,

$$(1+F)\xi_1' = (1-F)\xi_1 + \frac{G_r}{(1+G)}\xi_2 + \frac{G_m}{(1+H)}\xi_3. \tag{31}$$

Equations (28) to (30) can be written in matrix form as,

$$\begin{pmatrix}\xi_1'\\ \xi_2'\\ \xi_3'\end{pmatrix} = \begin{pmatrix}\frac{(1-F)}{(1+F)} & A_1 & A_2\\ 0 & \frac{(1-G)}{(1+G)} & 0\\ 0 & 0 & \frac{(1-H)}{(1+H)}\end{pmatrix}\begin{pmatrix}\xi_1\\ \xi_2\\ \xi_3\end{pmatrix}. \tag{32}$$

In matrix above, A_1 and A_2 are as

$$A_1 = \frac{G_r}{(1+F)(1+G)},\ A_2 = \frac{G_m}{(1+F)(1+H)}.$$

According to stability analysis of the finite difference scheme, the modulus of each eigen value of the amplification matrix does not exceed unity. Since the matrix equation (32) in triangular form, the eigen values are its diagonal elements. Therefore, the eigen values of the amplification matrix are $(1-F)/(1+F)$, $(1-G)/(1+G)$ and $(1-H)/(1+H)$. Since the real part of F is greater than or equal to zero, thus $(1-F)/(1+F) \le 1$, similarly, $(1-G)/(1+G) \le 1$ and $(1-H)/(1+H) \le 1$. Hence, the finite difference scheme is unconditionally stable. The Crank-Nicolson scheme has a truncation error of $O(\Delta t^2 + \Delta R^2)$, i.e. the temporal truncation error is significantly small. It tends to zero as Δt and ΔR tend to zero. So, the scheme is compatible. Stability and compatibility ensure convergence.

4. Results and Discussion

In order to explain the significance of the study, a representative set of numerical results for different parameters like, Casson fluid parameter (γ), magnetic field parameter (M), Prandtl

number (Pr) and chemical reaction parameter (K_0) are shown graphically in Figures 1 to 4. It is observed from Figure 1, that the effect of increasing values of the parameter M results in decreasing the fluid velocity. It is due to the application of transverse magnetic field that acts as Lorentz's force which retards the flow. Casson parameter (γ) is inversely proportional to the yield stress and it is observed that for the large value of Casson parameter, the fluid is close to the Newtonian fluid where the velocity is less than the Non-Newtonian fluid. Therefore, the effect of Casson parameter (γ) on velocity profile for unsteady motion is clearly exhibited in Figure 2. The effect of increasing values of γ is to increase the velocity. It means, if increasing values of the Casson parameter then decreasing yield stress (the fluid behaves as Newtonian fluid as Casson parameter becomes large) suppress the velocity field. Therefore, it is important to note that an increase in Casson parameter makes the velocity boundary layer thickness shorter. It is further observed from this graph that when the Casson parameter γ is large enough, the non- Newtonian behaviors disappear, and the fluid purely behaves like a Newtonian fluid. Thus, the velocity boundary layer thickness for Casson fluid is larger than the Newtonian fluid. It occurs because of plasticity of Casson fluid.

When Casson parameter is decreases then the plasticity of the fluid increases, which cause the increment in velocity boundary layer thickness. It is deduced that when chemical reaction parameter K_0 is increased then the velocity is decreased (Figure 3). Further from Figure 4, the numerical results show that the effect of increasing values of Prandtl number results in a decreasing velocity. It is noticed that an increase in the Prandtl number results a decrease of the thermal boundary layer thickness and in general lower average temperature within the boundary layer. The reason is that smaller values of P_r are equivalent to increase in the thermal conductivity of the fluid and therefore, heat is able to diffuse away from the heated surface more rapidly for higher values of P_r. Hence in the case of smaller Prandtl number as the thermal boundary layer is thicker and the rate of heat transfer is reduced.

Skin friction (τ) is given in Table 1. The value of Skin friction increases with the increase in the magnetic field parameter, Prandtl number, Schmidt number and chemical reaction parameter while its value decreases with the increases in the Casson parameter. Nusselt number (Nu) is given in Table 2. The value of Nusselt number increases with the increase in the Prandtl number. Sherwood number is given in Table 3. The value of Sherwood number increases with the increase in the chemical reaction parameter.

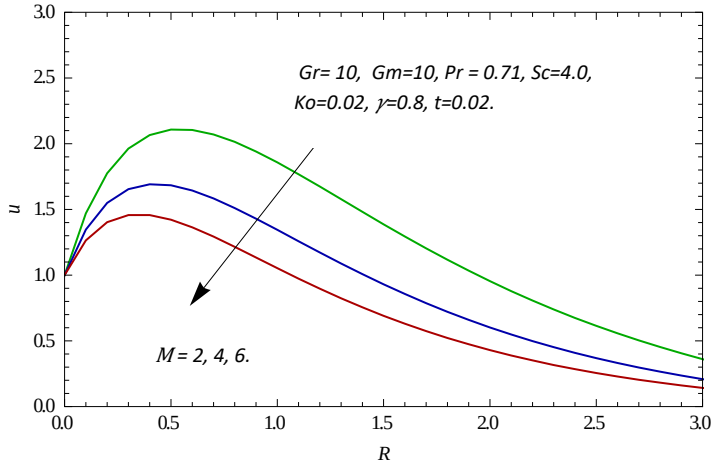

Figure 1. Velocity u for different values of M

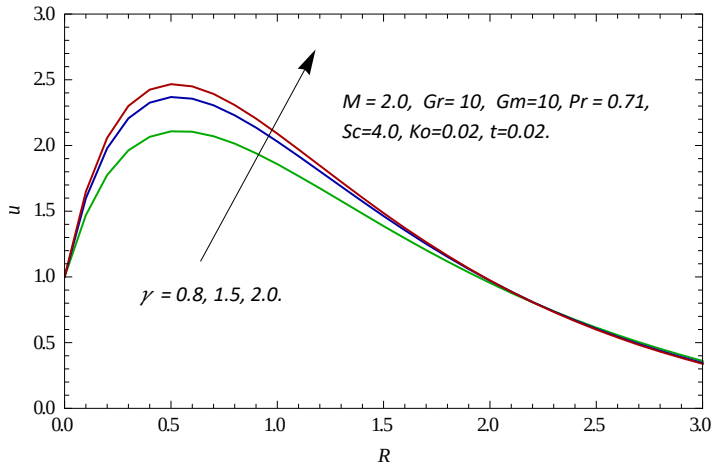

Figure 2. Velocity u for different values of γ

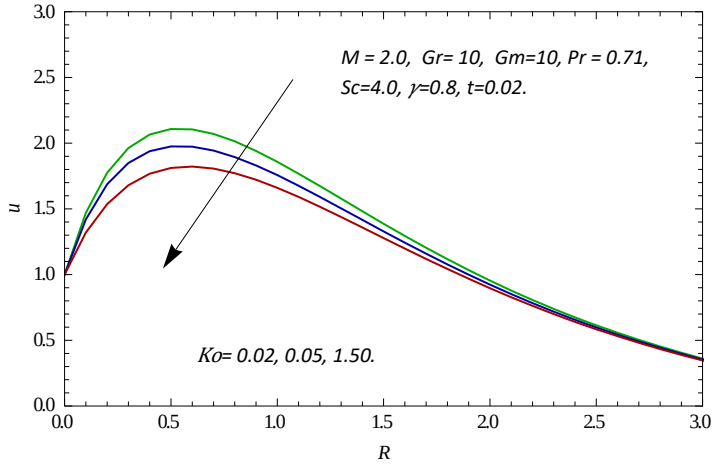

Figure 3. Velocity u for different values of K_0

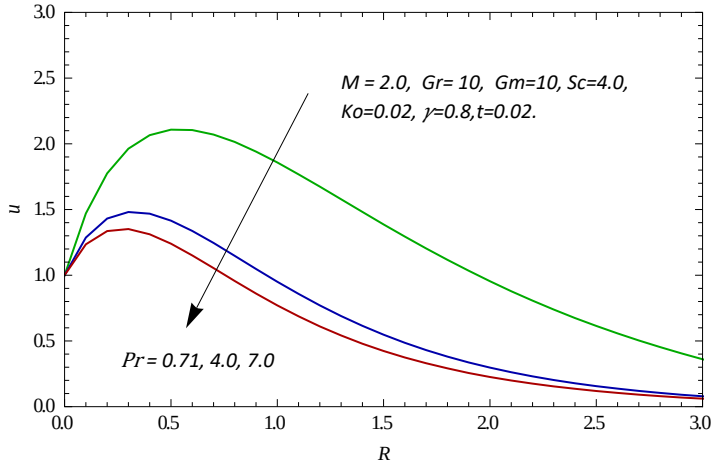

Figure 4. Velocity u for different values of Pr

Table 1. Skin friction τ for different Parameters

M	Pr	Sc	Gm	Gr	K_0	γ	t	τ
2.00	0.71	4.00	10.00	10.00	0.02	0.8	0.02	−4.7033
4.00	0.71	4.00	10.00	10.00	0.02	0.8	0.02	−3.4644
6.00	0.71	4.00	10.00	10.00	0.02	0.8	0.02	−2.6451
2.00	0.71	4.00	10.00	10.00	0.02	0.8	0.02	−4.7033
2.00	4.00	4.00	10.00	10.00	0.02	0.8	0.02	−2.8731
2.00	7.00	4.00	10.00	10.00	0.02	0.8	0.02	−2.3569
2.00	0.71	4.00	10.00	10.00	0.02	0.8	0.02	−4.7033
2.00	0.71	4.00	10.00	10.00	0.05	0.8	0.02	−4.2019
2.00	0.71	4.00	10.00	10.00	1.5	0.8	0.02	−3.2030
2.00	0.71	4.00	10.00	10.00	0.02	0.8	0.02	−4.7033
2.00	0.71	4.00	10.00	10.00	0.02	1.5	0.02	−5.9819
2.00	0.71	4.00	10.00	10.00	0.02	2.0	0.02	−6.4903

Table 2. Nusselt number Nu for different Parameters

M	Pr	Sc	Gm	Gr	K_0	γ	t	Nu
2.00	0.71	4.00	10.00	10.00	0.02	0.8	0.02	2.1077
2.00	4.00	4.00	10.00	10.00	0.02	0.8	0.02	3.7846
2.00	7.00	4.00	10.00	10.00	0.02	0.8	0.02	4.6439

Table3. Sherwood number Sh for different Parameters.

M	Pr	Sc	Gm	Gr	K_0	γ	t	Sh
2.00	0.71	4.00	10.00	10.00	0.02	0.8	0.02	6.1389
2.00	0.71	4.00	10.00	10.00	0.05	0.8	0.02	8.0570
2.00	0.71	4.00	10.00	10.00	1.5	0.8	0.02	17.5928

5. Conclusions

The numerically investigation has been done for the MHD Casson fluid flow model under consideration by transforming the governing non-linear partial differential equations into non-dimensional form. The MHD Casson fluid flow model consists of equations of motion, diffusion and energy equation. The governing equations of non-dimensional form of flow model have been solved numerically using Crank-Nicolson implicit finite difference method. To investigate the solutions obtained, standard sets of the values of the parameters have been taken. It is observed the velocity of the fluid flow is increased with increasing values of γ. In the other hand, the velocity of fluid retards with increased the value of magnetic field parameter, chemical reaction parameter and Prandtl number. The numerically result obtained for Skin friction, Nusselt number and Sherwood number is discussed with the help of Tables 1, 2 and 3. It is concluded that, the Skin friction increases with the increase in the magnetic field parameter, Prandtl number, Schmidt number and chemical reaction parameter while, it decreases with increased the value of Casson parameter. The Nusselt number increases with the increase in the Prandtl number. The Sherwood number increases with the increase in the chemical reaction parameter. We found that the numerically result obtained is in concurrence with the actual flow behavior of MHD Casson fluid.

Acknowledgement

We are thanks to the honorable Editor-in-Chief, Professor Aliakbar M. Haghighi; the reviewers; each member of the Editorial Board; and the staff of the Journal "Application and Applied Mathematics" for their valuable comments and suggestions which helped in improving the manuscript.

REFERENCES

Animasaun, I.L., Adebile, E.A. and Fagbade, A.I. (2016). Casson fluid flow with variable thermo-physical property along exponentially stretching sheet with suction and exponentially decaying internal heat generation using the homotopy analysis method, Journal of the Nigerian Mathematical Society, Vol. 35, pp.01–17.

Afikuzzaman, M., Ferdows, M. and Alam, M.M. (2014). Unsteady MHD Casson fluid flow through a parallel plate with Hall current, Procedia Engineering, Vol. 105, pp. 287-293.

Carnahan, B., Luther, H.A. and Wilkes, J.O. (1969). *Applied Numerical Methods*, John Wily and Sons, New York.

Chamkha, A.J., Abbasbandy, S. and Rashad, A.M. (2013). Radiation effects on mixed convection about a cone embedded in a porous medium filled with a nano fluid. Meccanica, Vo. 48, pp. 275-285.

Das, B. and Batra, R.L. (1993). Secondary flow of a Casson fluid in a slightly curved tube, Int. J. Non-Linear Mechanics, Vol. 28, No.5, pp.567-577.

Eugen Magyari and Chamkha, A.J. (2010). Combined effect of heat generation or absorption and first-order chemical reaction on micropolar fluid flows over a uniformly stretched permeable surface: The full analytical solution International Journal of Thermal Sciences vol. 49, NO. 9, PP. 1821-1828

Ghalambaz, M., Mehryan, S.A.M. and Izadpanahi, E. (2019). MHD natural convection of Cu–Al2O3 water hybrid nanofluids in a cavity equally divided into two parts by a vertical flexible partition membrane. J Therm Anal Calorim, Vol.138, pp. 1723–1743.

Hazem, A.A and Mohamed E.S.A. (2010). Transient MHD Couette flow of a Casson fluid between parallel plates with heat transfer, Italian journal of pure and applied mathematics, Vol. 27, pp. 19-38,

Husein, A. Alzgool, Hamzeh, T., Alkasasbeh, Sana A., Zain Al-houri and Mohammed, Z.S. (2019). Numerical solution of heat transfer in MHD mixed convection flow micropolar Casson fluid about solid sphere with radiation effect, International Journal of Engineering Research and Technology, Vol. 12, No. 4, pp. 519-529.

Kataria, H. R. and Patel H.R. (2018). Heat and mass transfer in magnetohydrodynamic (MHD) Casson fluid flow past over an oscillating vertical plate embedded in porous medium with ramped wall temperature, Propulsion and Power Research, Vol. 7, No. 3, pp. 257–267.

Kumar, G., kumar, A., Misra, M. K. and Srivastava,V. (2019). Chemical reaction effect on MHD flow past an impulsively started vertical cylinder with variable temperature and mass diffusion, Journal of Science and Arts, Vol. 47, No. 2, pp. 513-522.

Kumar, G. and Bansal, A. (2019). Unsteady flow past on vertical cylinder in the presence of an inclined magnetic field and chemical reaction, Analele Universităţii "Eftimie Murgu" Reşiţa Anul, Vol. 23 , No. 1, pp. 305-319.

Mustafa, M., Hayat, T., pop, I. and Aziz, A. (2011). Unsteady boundary layer flow of a casson fluid due to an impulsively started moving flate plate. Heat Transfer- Asian Res, Vol. 40, No. 6, pp. 563-576.

Pramanik, P. (2014). Casson fluid flow and heat transfer past an exponentially porous stretching surface in presence of thermal radiation, Ain Shams Engineering Journal, Vol. 5, pp. 205–212.

Pushpalatha, K., Sugunamma, V., Ramana Reddy, J. V. and Sandeep, N. (2016), Heat and mass transfer in unsteady MHD Casson fluid flow with convective boundary conditions, International Journal of Advanced Science and Technology, Vol. 91, pp. 19-38.

Ramana Reddy, J.V., Sugunamma,V. and Sanddep, N. (2016). Effect of aligned magnetic field on Casson fluid flow past a vertical oscillating plate in porous medium, Journal of Advanced Physics, Vol. 5, No. 4, pp.295-301.

Rajput, U.S. and Kumar, G. (2018). Rotation and radiation effects on MHD flow past an inclined plate with variable wall temperature and mass diffusion in the presence of Hall current, Applications and Applied Mathematics: An International Journal (AAM), Vol. 13, No. 1, pp. 484-495.

Rajput, U.S. and Kumar, G. (2016).Unsteady MHD flow past an impulsively started inclined plate with variable temperature and mass diffusion in the presence of Hall current, Applications and Applied Mathematics: An International Journal (AAM), Vol. 11, No. 2, pp. 693-703.

Rajput, U. S and Kumar G. (2019). Effects of radiation and chemical reaction on MHD flow past a vertical plate with variable temperature and mass diffusion, Journal of Naval Architecture and Marine Engineering, Vol. 16, pp 99-108.

Rajput, U. S and Kumar G. (2016). Unsteady MHD flow in porous media past over exponentially accelerated inclined plate with variable wall temperature and mass transfer along with Hall current. International Journal of Engineering, Science and Technology, Vol. 8, No. 2, pp. 1-10.

Takhar, H., Chamkha, A. and Nath, G. (2000). Combined heat and mass transfer along a vertical moving cylinder with a free stream. Heat and Mass Transfer 36, pp. 237–246.

Takhar, H.S., Chamkha, A.J. and Nath, G. (2001). Unsteady three-dimensional MHD-boundary-layer flow due to the impulsive motion of a stretching surface. Acta Mechanica, Vol. 146, 59–71.

Vijayaragavan, R. and Karthikeyan, S. (2018). Hall current effect on chemically reacting MHD Casson fluid flow with Dufour effect and thermal radiation, Asian Journal of Applied Science and Technology, Vol. 2, No. 2, pp.228-245.

Walwander, W.P., Chen, T.Y. and Cala, D.F. (1975). An approximate Casson fluid model for tube flow of blood, Biorheology, Vol. 12, pp.111-119.

Wahiduzzaman, M., Musa Miah M., Babul Hossain M., Johora F. and Mistri, S. (2014). MHD Casson fluid flow past a non-isothermal porous linearly stretching sheet, Prog. Nonlinear Dynamics Chaos, Vol. 2, No. 2, pp.61-69.